Electronic Supplementary Information

In situ post-modification of substoichiometric 2D conjugated MOFs to boost ethylene selectivity in electrocatalytic CO_2 reduction

Yijun Li,‡[a] Jianning Lv,‡[a] Shuai Li,[a] Lu Dai,[a] Bo Wang,[a,c] and Pengfei Li*[a,b]

[a]Frontiers Science Center for High Energy Material, Key Laboratory of Cluster Science, Ministry of Education, Beijing Key Laboratory of Photoelectronic/Electrophotonic Conversion Materials, School of Chemistry and Chemical Engineering, Beijing Institute of Technology, Beijing 100081, P. R. China

[b]Advanced Research Institute of Multidisciplinary Science, Beijing Institute of Technology, Zhuhai, No.6, Jinfeng Road, Tangjiawan, Zhuhai, 519088, P. R. China

[c]Advanced Technology Research Institute (Jinan), Beijing Institute of Technology, Jinan, 250300, P. R. China

E-mail: lipengfei@bit.edu.cn

Table of contents

Section 1. Materials and Characterization

Copper nitrate hemipentahydrate ($Cu(NO_3)_2 \cdot 2.5H_2O$) was purchased from Macklin chemical. 2,3,6,7,10,11-triphenylenehexol and tetrafluoroterephthalonitrile were purchased from Energy Chemical Co., Ltd. Other chemicals were supplied by Energy Chemical Co., Ltd. and Beijing Chemical Reagent Company, which were directly used without further purification.

^{1}H NMR spectra were measured on a Bruker ARX-400 NMR spectrometer with tetramethylsilane (TMS) as the internal standard. The solid-state ^{13}C NMR and ^{19}F NMR spectra were measured on a Bruker ARX-700 NMR spectrometer. Powder X-ray diffraction (PXRD) was recorded on a Rigaku MiniFlex 600 diffractometer using Cu Kα X-ray source with 40 kV voltage and 50 mA current. Fourier transform infrared (FT-IR) spectra were performed on Bruker ALPHA spectrometer in the range of 400~4000 cm^{-1}. The elemental analysis (EA) was performed on an Elementar Vario MICRO analyzer. The inductively coupled plasma atomic emission spectrometry (ICP-AES) was measured with Prodigy 7. N_2 sorption isotherms were carried out at 77 K on a Quantachrome Instrument Autosorb-iQ after degassed under vacuum at 120 ^{o}C for 12 h. The pore size distributions were determined by non-local density function theory (NLDFT). Thermogravimetric analysis (TGA) was conducted on a NETZSCH Proteus STA 449F5 analyzer by heating the sample within the temperature range of 35~800 ^{o}C under N_2 atmosphere at a heating rate of 5 ^{o}C /min. Scanning electron microscopy (SEM) images were obtained from a JEOL model JSM-7500F scanning electron microscope. Transmission electronic microscopy (TEM) was carried out with a JEOL model JEM-2100 microscope at 200 kV. X-ray photoelectron spectroscopy (XPS) was performed by using Thermo scientific ESCALAB 250Xi with Al Kα radiation. The water contact angle was measured by the sessile drop method using an optical surface analyzer (OSA200, Ningbo NB Scientific Instruments).

Section 2. Experimental Section

General procedures for the measurement of conductivity:

The powder of 2D *c*-MOFs was first pressed into pellets under 3 MPa for 60 s. The resultant pellet has a radius of 6.5 mm and a thickness of ~0.5 mm. Furthermore, the conductivity was measured by a four-point collinear probe with a probe distance of 1 mm by RTS-9 digital four-probe tester at room temperature.

The digestion for procedures for *def*-Cu-HHTP-TFPN:

The *def*-Cu-HHTP-TFPN sample after Soxhlet extracted was immersed in 1 mL of 12 M HCl aqueous solution and stirred at 300 rpm for 24 hours. The digested mixture was centrifuged at 8000 rpm for 5 minutes. The resulting supernatant was used for further testing.

CO_2 electrochemical reduction (CO_2RR) tests:

The reduction of CO_2 was conducted in an H-type cell with two compartments separated by a Nafion-117 membrane and tested by an electrochemical workstation (CHI 760E). Each compartment contained a CO_2-saturated $KHCO_3$ (30 mL, 0.1 M) as the electrolyte. LSV and electrolysis were performed in a three-electrode system using Pt foil as the counter electrode and Ag/AgCl electrode as the reference electrode. The working electrode was prepared as follows: 5 mg of catalyst and 40 μL 5 wt% Nafion were dispersed in 0.5 mL isopropanol and sonicated for 30 min. Then 10 μL of the resulting ink was dropped onto the surface of a glass carbon electrode (GCE) with a disk diameter of 5 mm to form the working electrode. All gas-phase products were detected by gas chromatography (GC-2014, Shimadzu) with TCD and FID detectors. Before electrolysis, pure CO_2 gas or Ar gas was bubbled into a 0.1 M $KHCO_3$ aqueous solution with stirring for 30 min to obtain CO_2-saturated $KHCO_3$ electrolyte. During the whole electrochemical test, CO_2 was kept in a purging state in the electrolyte. The CO_2RR performance was tested by using constant-current electrolysis. All potentials vs. Ag/AgCl reference electrode were converted to the reversible hydrogen electrode (RHE) using the formula:[1]

$$E\ (vs.\ RHE) = E\ (vs.\ Ag/AgCl) + 0.196\ V + 0.059 \times pH$$

(pH = 6.8 for CO_2 saturated 0.1 M $KHCO_3$)

The Faradaic efficiency of the gas product was calculated by the equation:

$$FE = \alpha nF/Q$$

(Where α is the number of the electrons transferred for a product, n is the total amount of the product (in moles), F is the Faraday constant, Q = it, i is the current in A, t is the running time in seconds).

The total turnover frequency (TOF) was calculated by the equation:

$$TOF = \frac{i \times FE}{N \times F \times n_{tot}}$$

Where i is the current, FE is the Faradaic efficiency for the product, N is the number of electrons in the half-reaction (N = 12 for the CO_2 to C_2H_4 conversion), F is the Faraday constant, and n_{tot} is the total moles of Cu active sites in the catalyst used in the electrolysis.

For the $^{13}CO_2$ labeling experiments, the above apparatus is used except that 0.1 M KCl as the electrolyte and the outlet gas was detected with a Hiden Analytical HPR 20 mass spectrometer.

Section 3 Supporting Figures and Tables

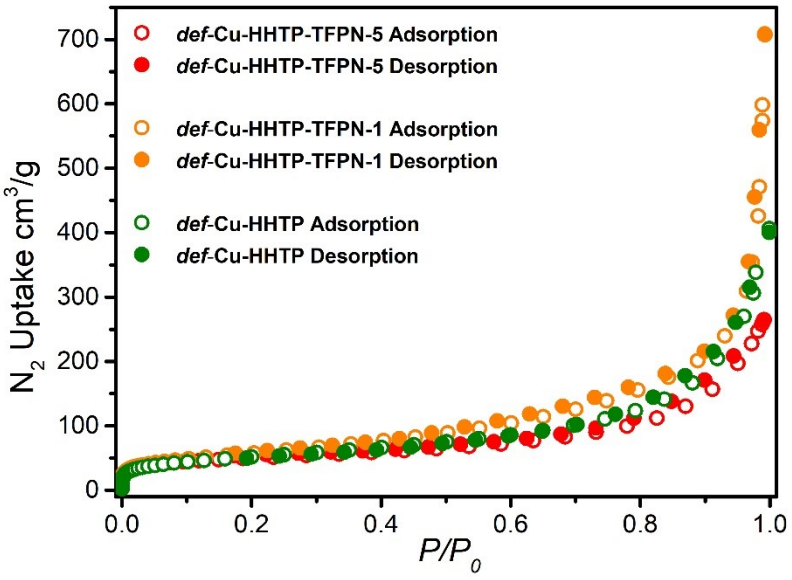

Figure S1. N_2 adsorption-desorption isotherms of *def*-Cu-HHTP, *def*-Cu-HHTP-TFPN-1, and *def*-Cu-HHTP-TFPN-5 at 77 K.

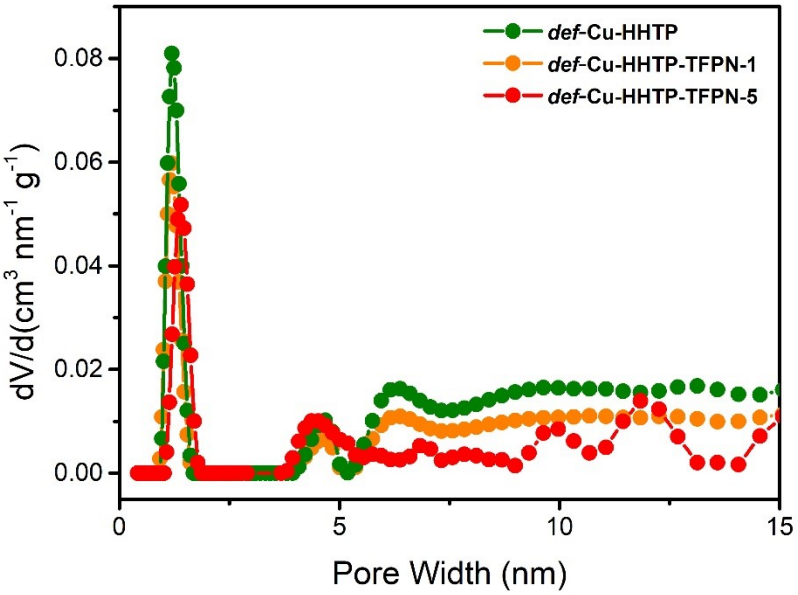

Figure S2. Pore width distributions of *def*-Cu-HHTP, *def*-Cu-HHTP-TFPN-1, and *def*-

Cu-HHTP-TFPN-5.

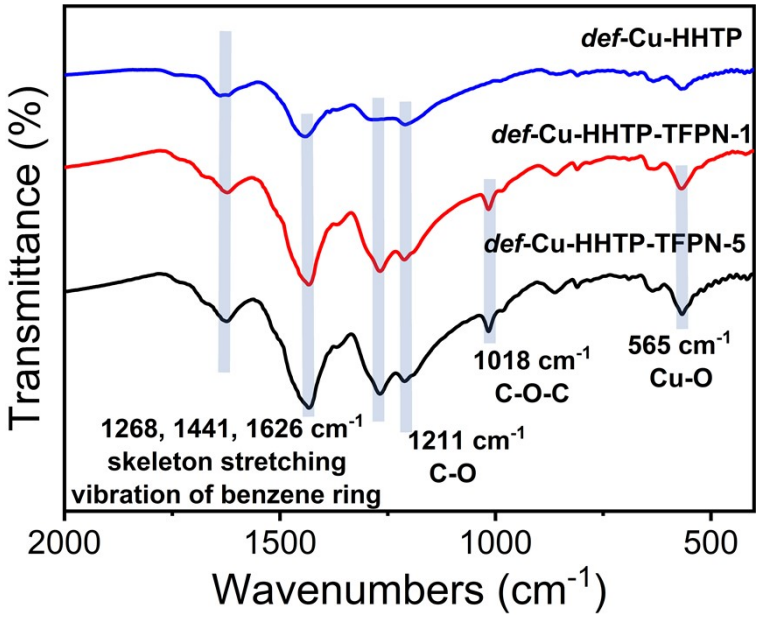

Figure. S3 The enlarged FT-IR spectra of *def*-Cu-HHTP, *def*-Cu-HHTP-TFPN-1, and *def*-Cu-HHTP-TFPN-5 from 400 cm^{-1} to 2000 cm^{-1}.

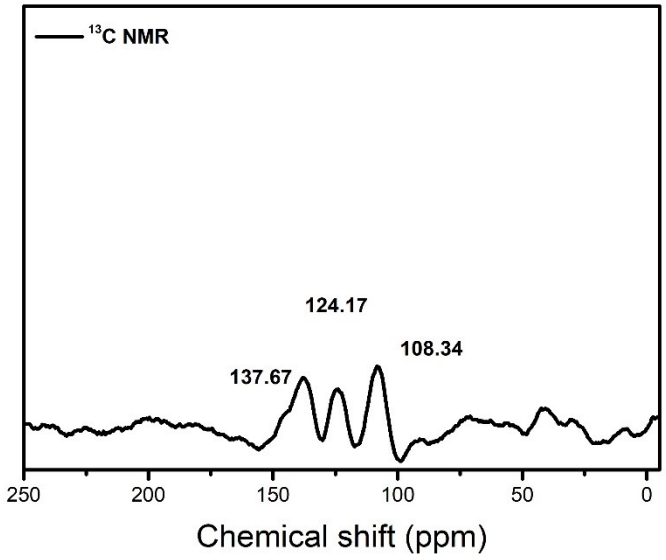

Figure S4. Solid-state ^{13}C NMR spectrum of *def*-Cu-HHTP-TFPN-1 (700 MHz).

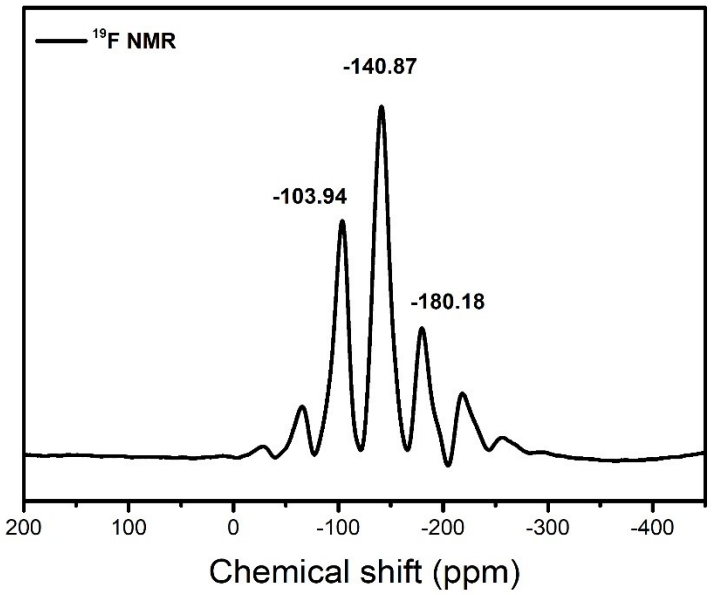

Figure S5. Solid-state ^{19}F NMR spectrum of *def*-Cu-HHTP-TFPN-1 (700 MHz).

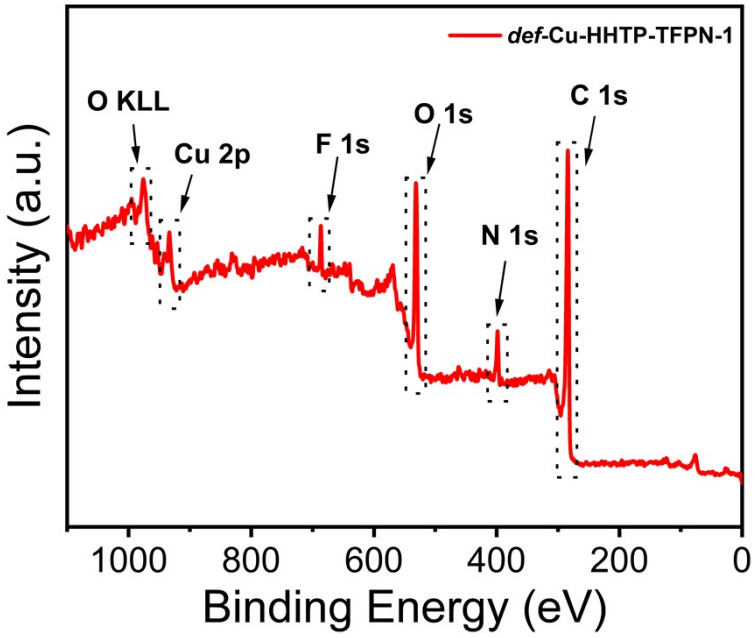

Figure S6. XPS survey spectrum of *def*-Cu-HHTP-TFPN-1.

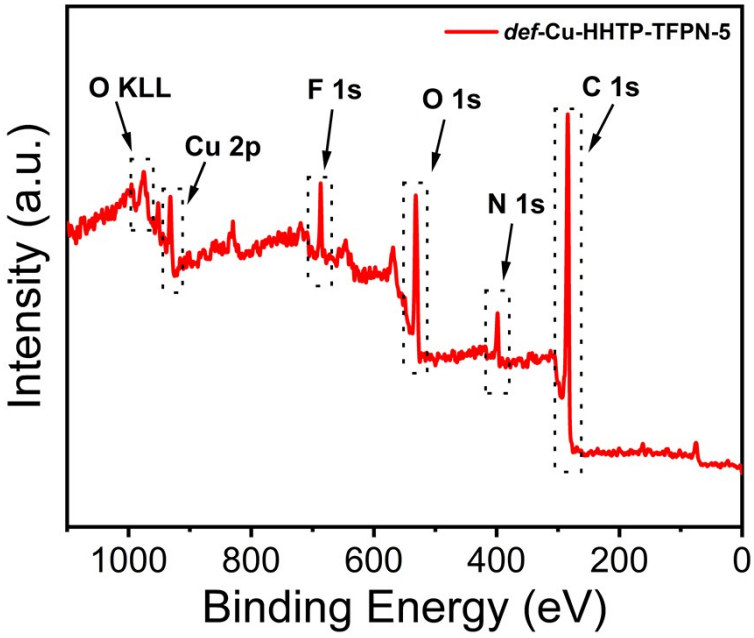

Figure S7. XPS survey spectrum of *def*-Cu-HHTP-TFPN-5.

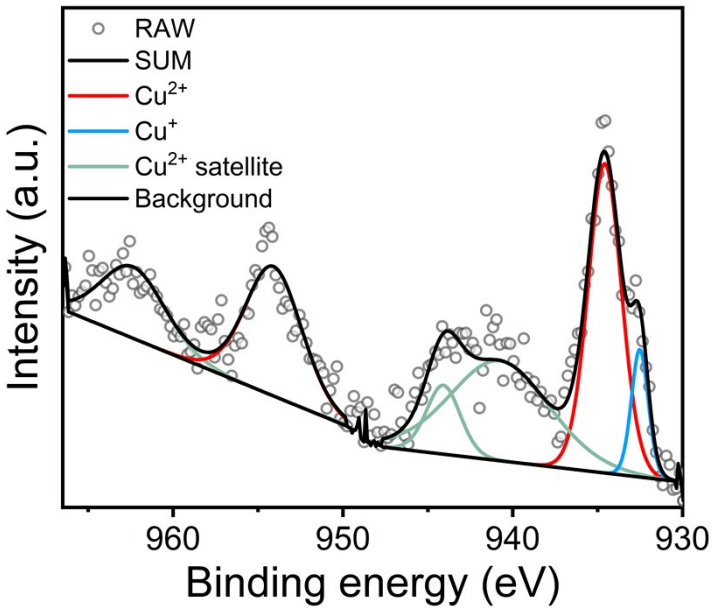

Figure S8. Cu 2p XPS spectrum of *def*-Cu-HHTP-TFPN-1.

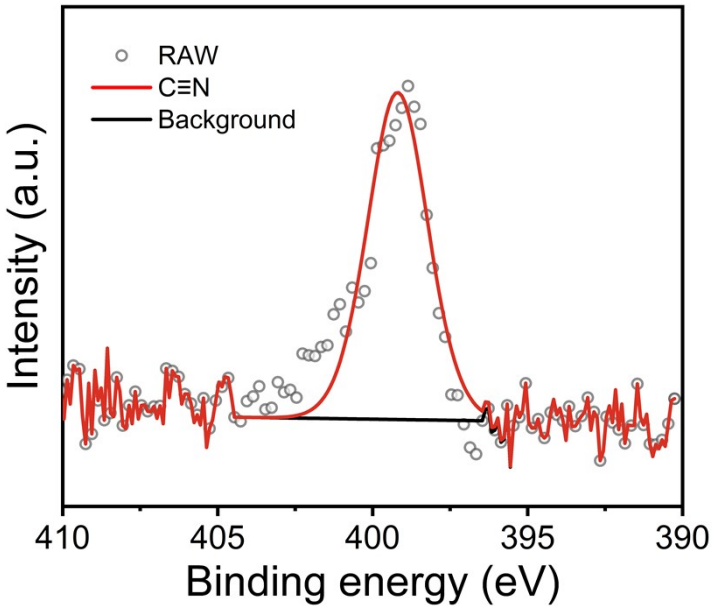

Figure S9. N 1s XPS spectrum of *def*-Cu-HHTP-TFPN-1.

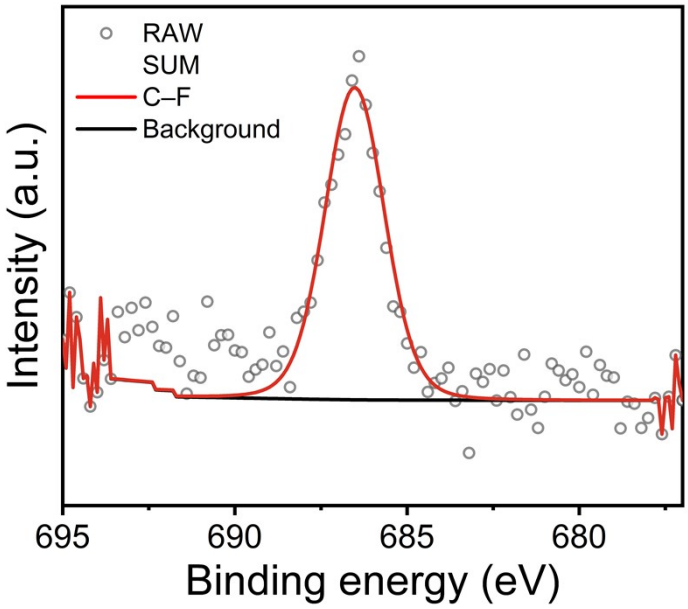

Figure S10. F 1s XPS spectrum of *def*-Cu-HHTP-TFPN-1.

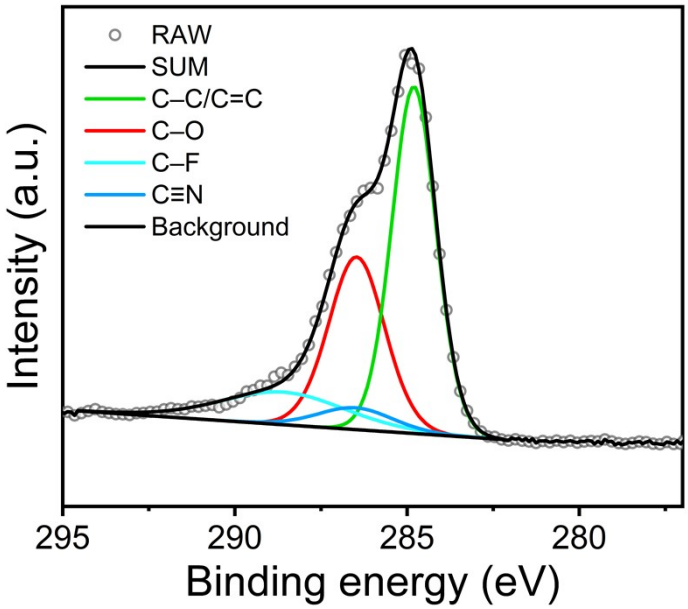

Figure S11. C 1s XPS spectrum of *def*-Cu-HHTP-TFPN-1.

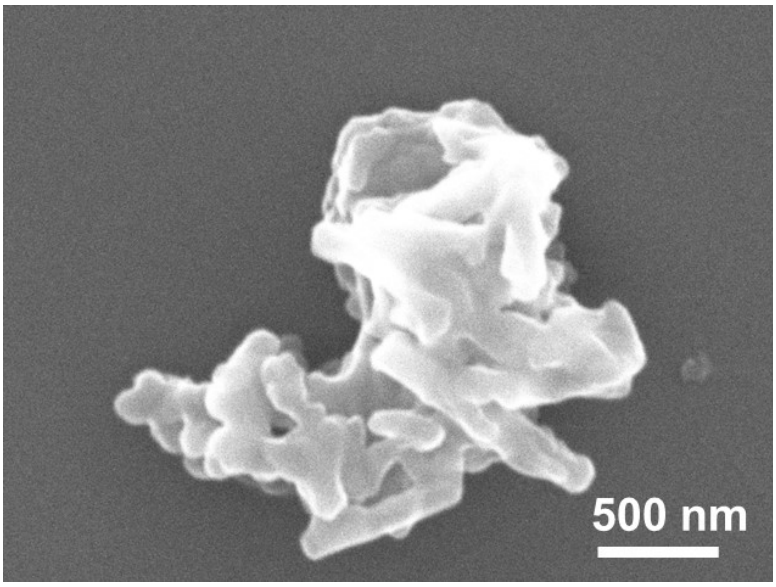

Figure S12. SEM image of *def*-Cu-HHTP-TFPN-1.

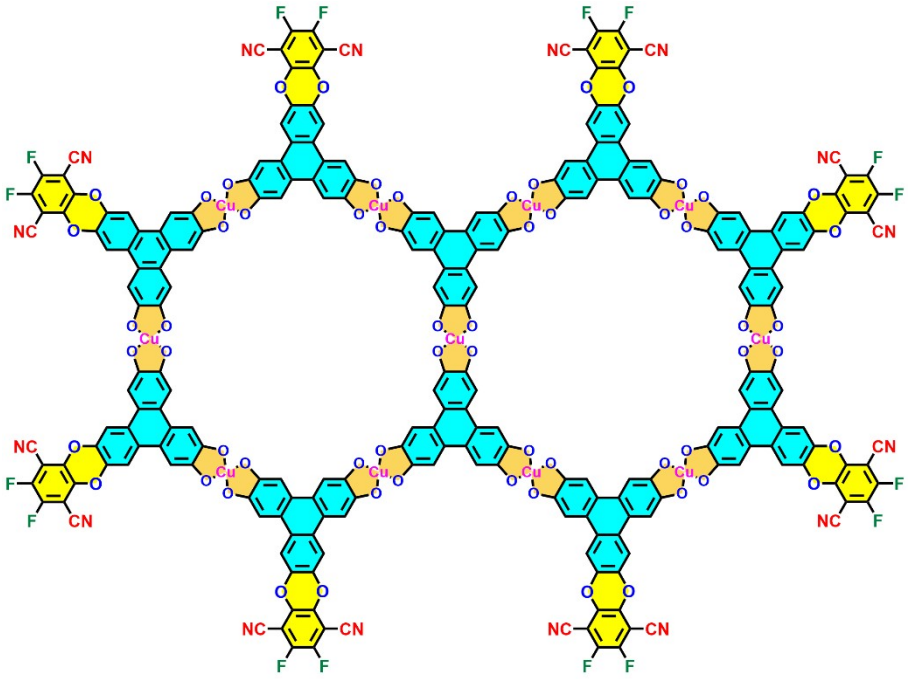

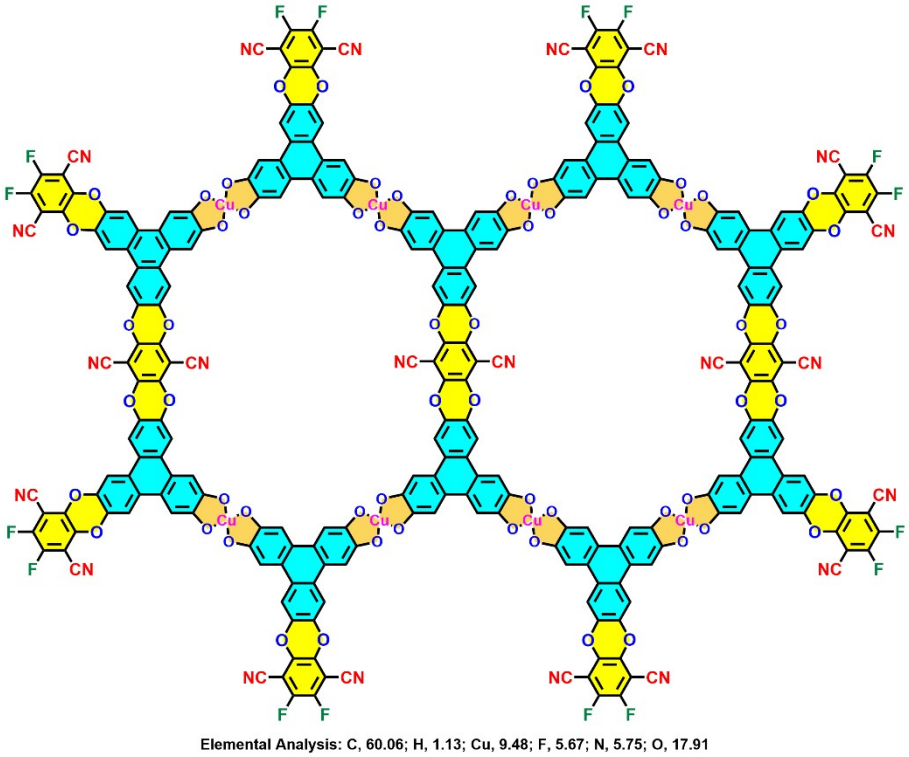

Figure S13. Structural models with different amounts of TFPN at specific points of *def*-Cu-HHTP-TFPN-x.

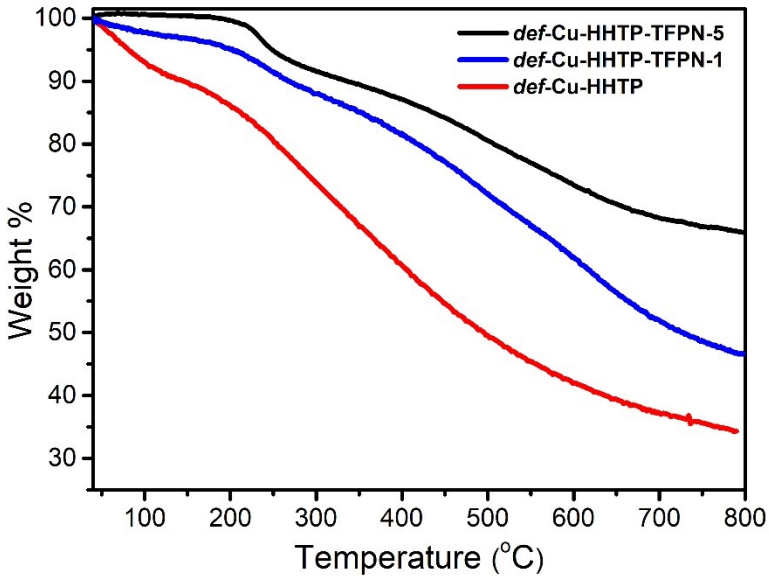

Figure S14. TGA curves of *def*-Cu-HHTP, *def*-Cu-HHTP-TFPN-1, and *def*-Cu-HHTP-TFPN-5.

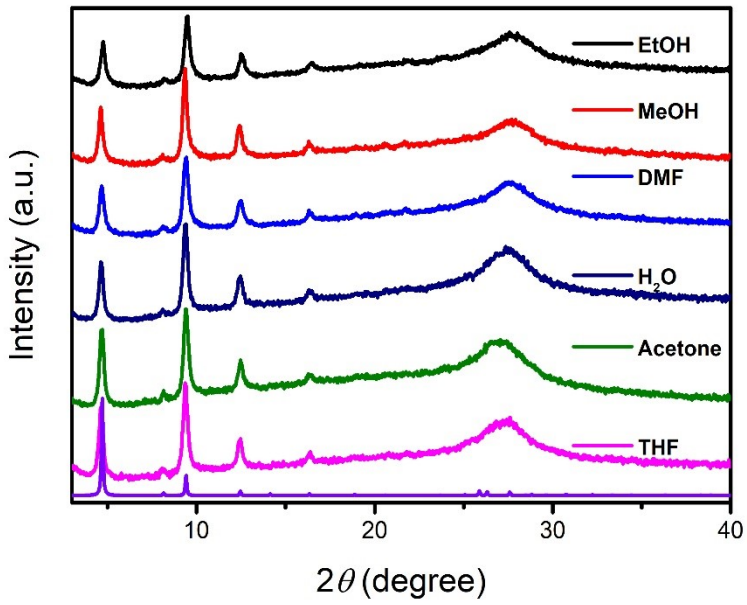

Figure S15. PXRD patterns of *def*-Cu-HHTP-TFPN-1 in different solvents.

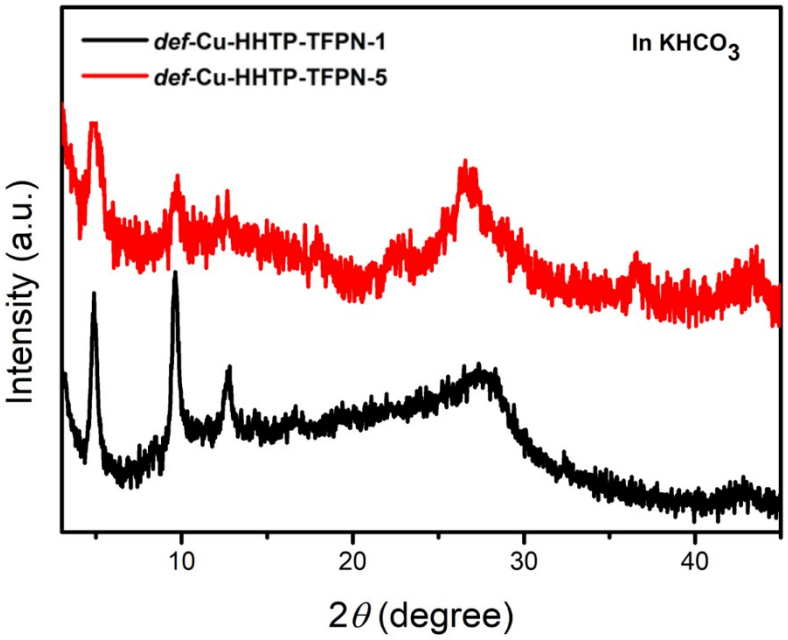

Figure S16. PXRD patterns of *def*-Cu-HHTP-TFPN-1 and *def*-Cu-HHTP-TFPN-5 in 0.1 M $KHCO_3$.

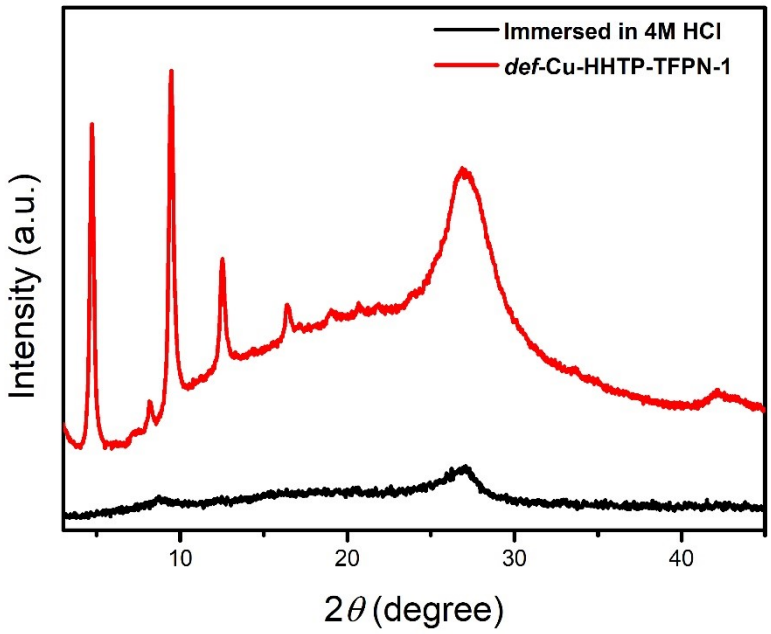

Figure S17. PXRD patterns of *def*-Cu-HHTP-TFPN-1 and its digested product.

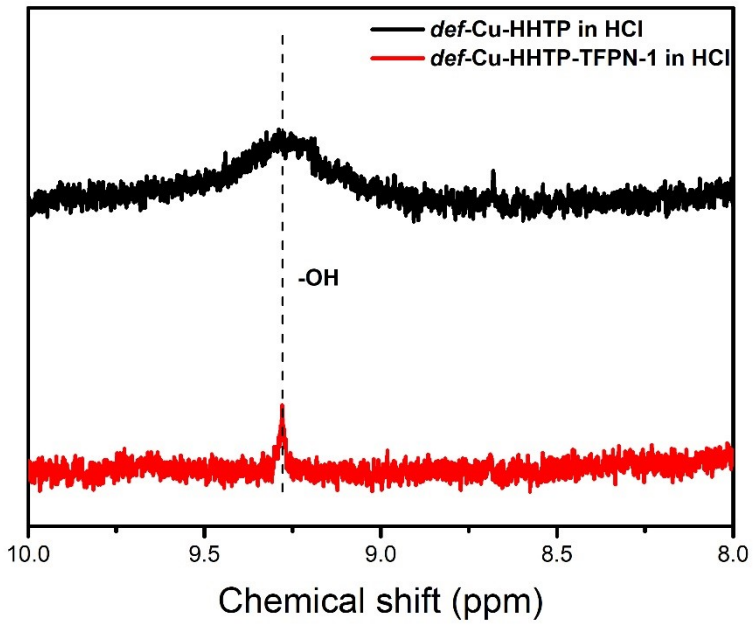

Figure S18. ^{1}H NMR spectrum of the digested product of *def*-Cu-HHTP and *def*-Cu-HHTP-TFPN-1 (DMSO-d_6, 400 MHz).

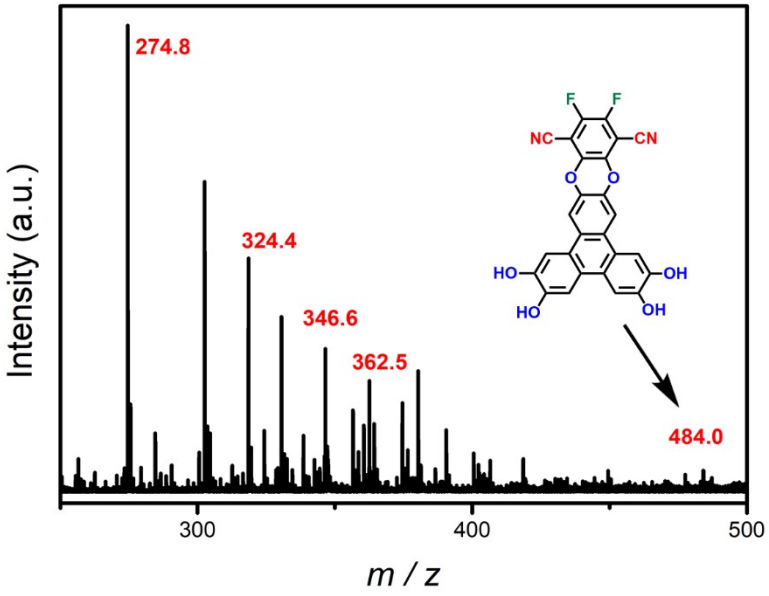

Figure S19. MALDI-TOF mass spectrum of the digested product of *def*-Cu-HHTP-TFPN-1.

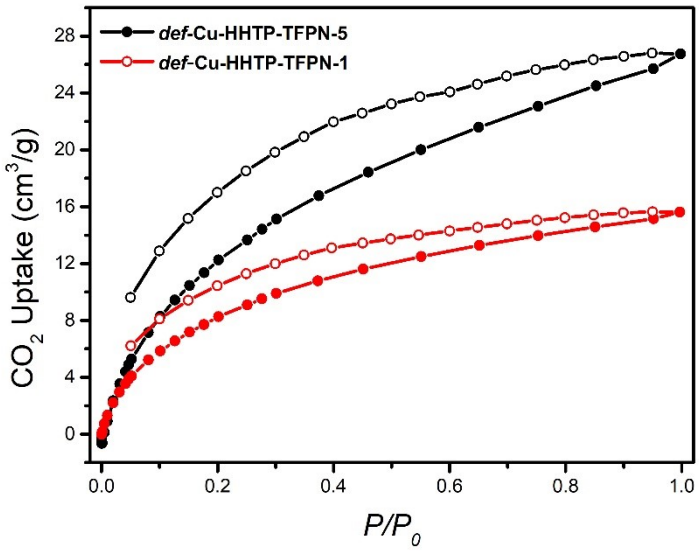

Figure S20. CO_2 adsorption isotherms of *def*-Cu-HHTP-TFPN-1 and *def*-Cu-HHTP-TFPN-5.

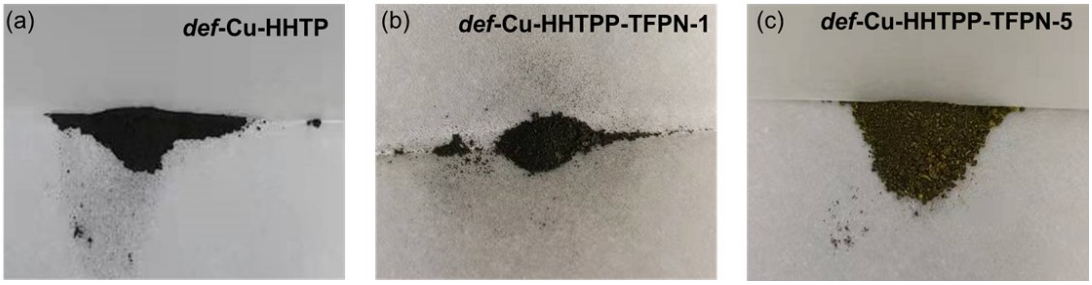

Figure S21. Photos of *def*-Cu-HHTP, *def*-Cu-HHTP-TFPN-1, and *def*-Cu-HHTP-TFPN-5.

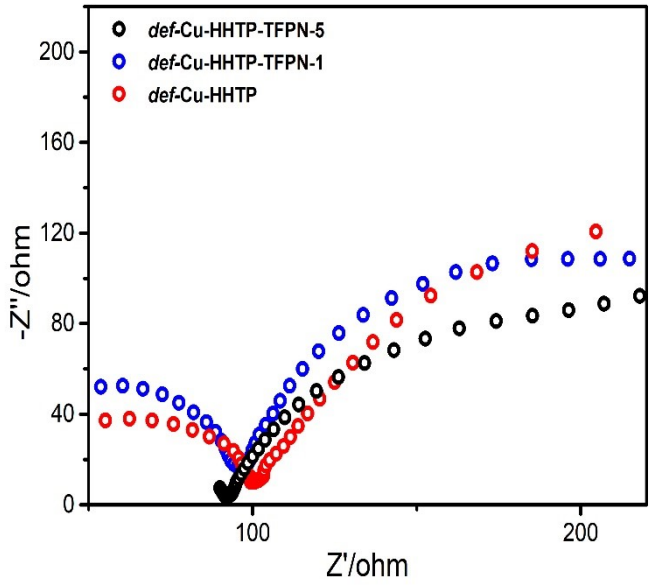

Figure S22. Impedance spectra of *def*-Cu-HHTP, *def*-Cu-HHTP-TFPN-1, and *def*-Cu-HHTP-TFPN-5.

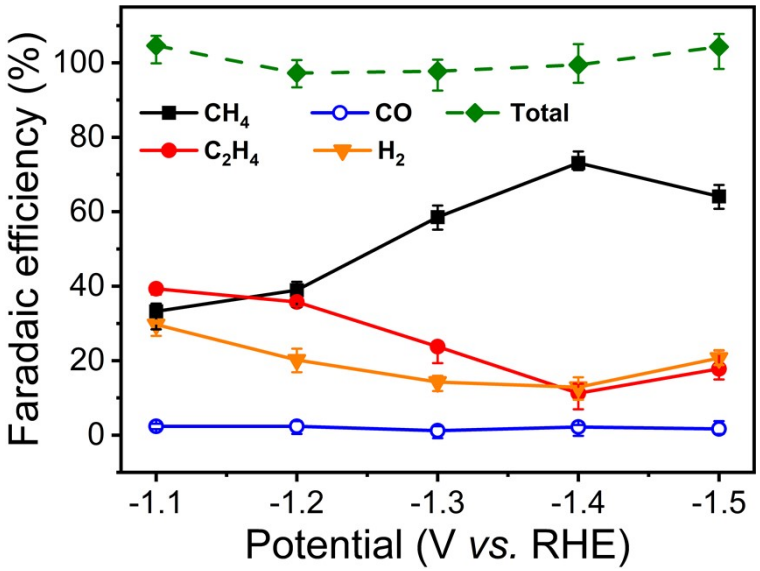

Figure S23. Potential dependent FE of different reduction products of *def*-Cu-HHTP.

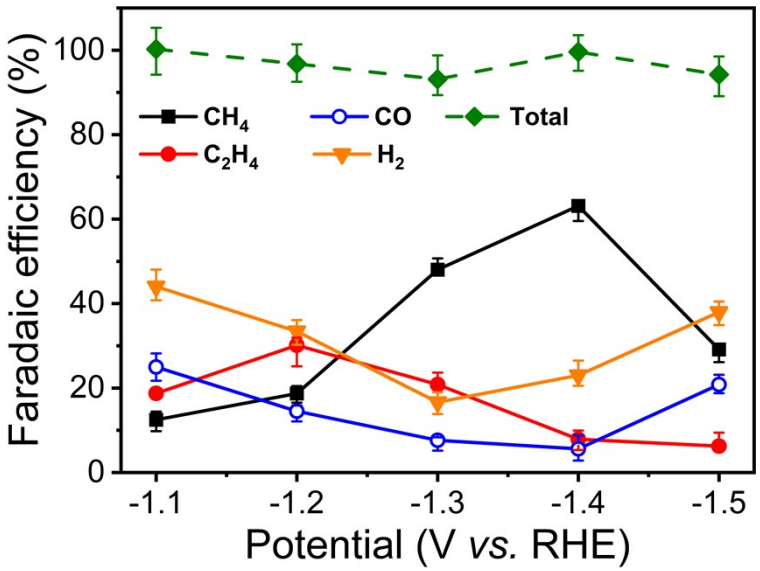

Figure S24. Potential dependent FE of different reduction products of *def*-Cu-HHTP-TFPN-5.

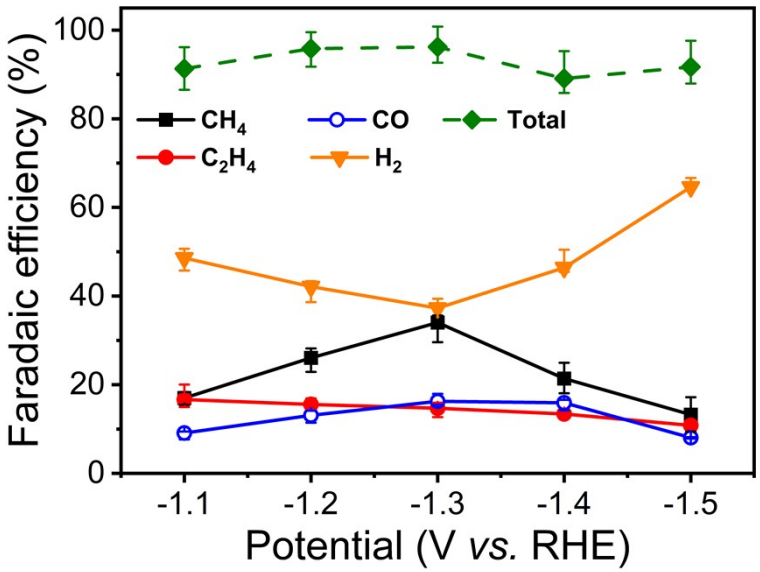

Figure S25 Potential dependent FE of different reduction products of pristine Cu-HHTP.

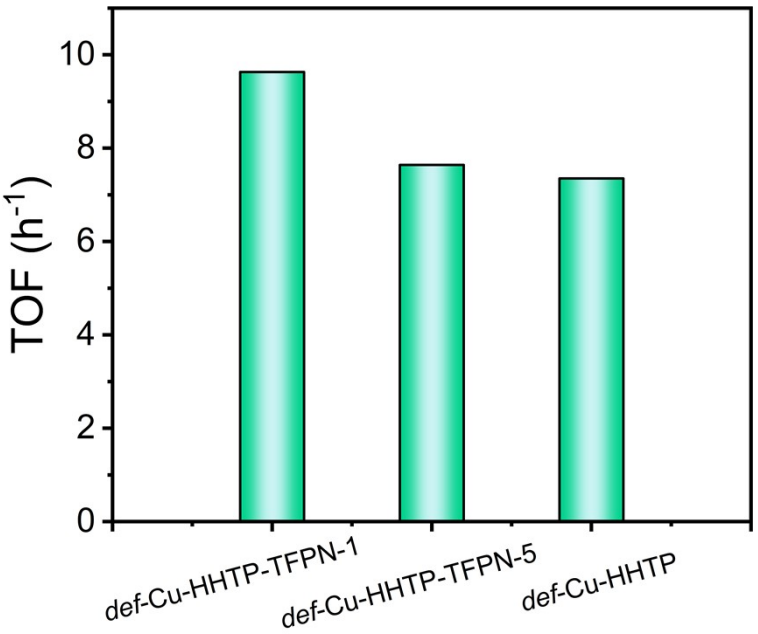

Figure S26 The TOF of *def*-Cu-HHTP, *def*-Cu-HHTP-TFPN-1, and *def*-Cu-HHTP-TFPN-5 at −1.2 V vs. RHE.

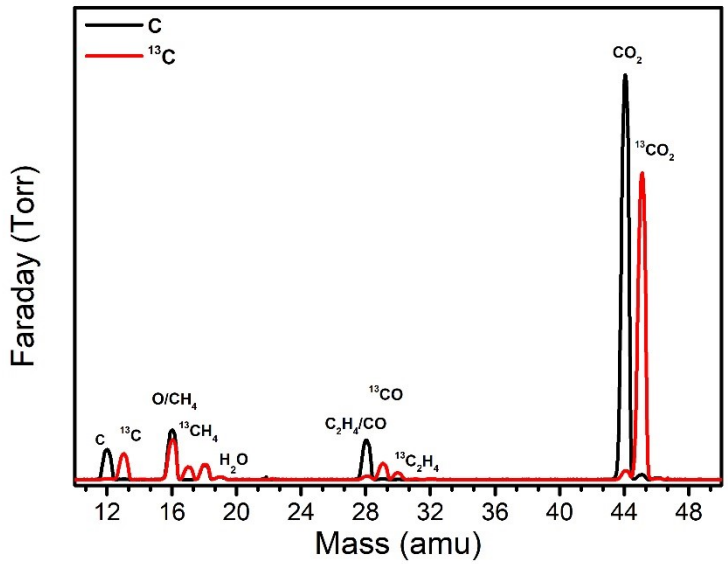

Figure S27. Mass spectra of the gaseous product with *def*-Cu-HHTP-TFPN-1 under CO_2RR electrolysis by using ^{13}C labeling CO_2 or ordinary CO_2.

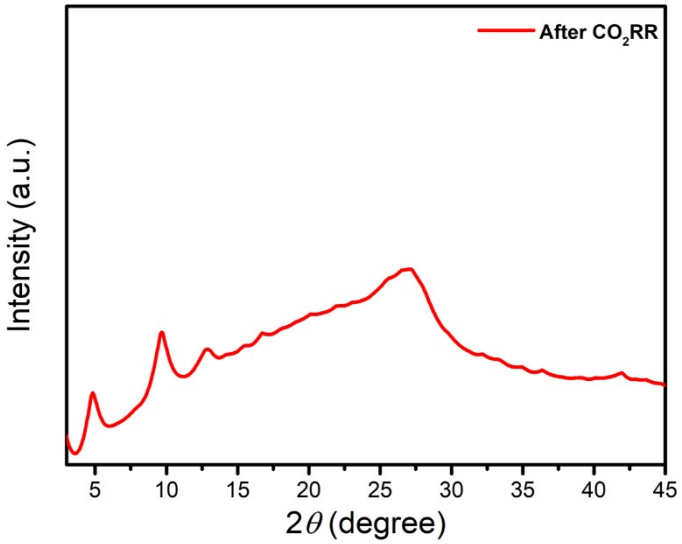

Figure S28. PXRD pattern of *def*-Cu-HHTP-TFPN-1 after electrolysis for 12 h.

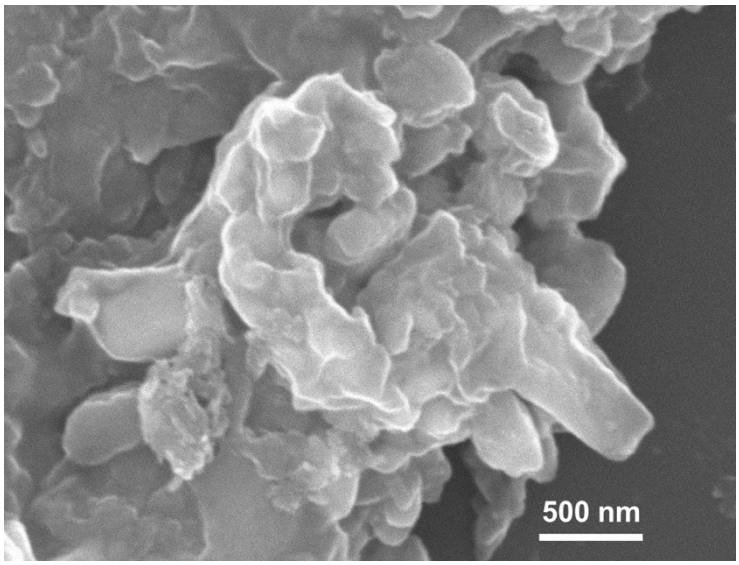

Figure S29. SEM image of *def*-Cu-HHTP-TFPN-1 after electrolysis for 12 h.

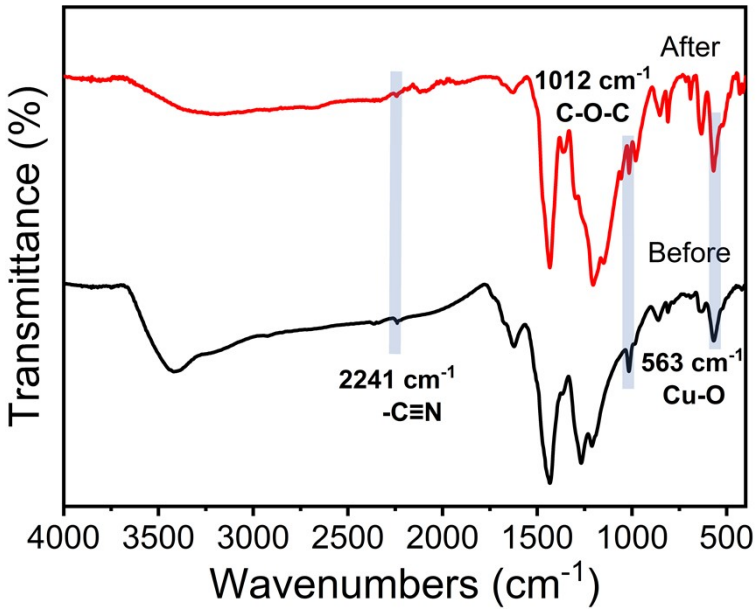

Figure S30 FT-IR spectra of *def*-Cu-HHTP-TFPN-1 before (black) and after (red) CO_2RR.

Table S1. Elemental content of *def*-Cu-HHTP and *def*-Cu-HHTP-TFPN-x (the contents of C, N, H were analyzed by elemental analysis and the contents of Cu were measured with ICP-AES).

	C (%)	N (%)	H (%)	Cu (%)
def-Cu-HHTP	53.04	0.81	2.42	17.87
def-Cu-HHTP-TFPN-1	57.10	4.63	1.90	14.32
def-Cu-HHTP-TFPN-5	61.10	6.98	1.59	10.87

Table S2. Comparison of the CO_2RR products and selectivity with other reported 2D *c*-MOFs electrocatalysts.

Catalysts	**Major Reduction Product**	**Selectivity (%)**	**Potential (V vs. RHE)**	**Ref.**
2D-*vc*-MOF(Cu)	CH_4	65	−1.4	*Angew. Chem. Int. Ed.* **2023**, *62*, e202217958.
$Cu_3(HHTP)_2$	CH_4	42.88	−1.3	*Molecular Catalysis*, **2023**, *540*, 113033.
Cu-THQ	CO	91	−0.45	*Adv. Mater.* **2021**, *33*, 2004393.
HATNA-Cu-MOF	CH_4	78	−1.5	*Angew. Chem. Int. Ed.* **2021**, *60*, 14473-14479.
$Cu_3(HHTQ)_2$	CH_3OH	53.6	−0.4	*Angew. Chem. Int. Ed.* **2021**, *60*, 16409.
NiPc-NiO_4	CO	98.4	−1.2	*Angew.Chem. Int. Ed.* **2021**, *60*,17108-17114.
Cu-DBC	CH_4	80	−0.9	*Nat. Commun.* **2021**, *12*, 6390.
CoPc-Cu-O	CO	85	-0.63	*J.Am.Chem.Soc*. **2020**, *142*, 21656−21669.
KB@$Cu_3(HITP)_2$	C_2H_4	70	−1.37	*Nat. Commun.* **2021**, *12*, 6823.
PcCu-Cu-O	C_2H_4	50	−1.2	*J. Am. Chem. Soc.* **2021**, *143*, 7242-7246.
***def*-Cu-HHTP-TFPN-1**	**C_2H_4**	**54**	**−1.2**	**This work**

Section 4. Supporting References

[1] Y. Liu, S. Li, L. Dai, J. Li, J. Lv, Z. Zhu, A. Yin, P. Li and B. Wang, *Angew. Chem. Int. Ed.*, 2021, **60**, 16409-16415